Applied Catalysis B: Environmental 166–167 (2015) 287–294

Contents lists available at ScienceDirect

Applied Catalysis B: Environmental

journal homepage: www.elsevier.com/locate/apcatb

Preparation of fiber-based plasmonic photocatalyst and its photocatalytic performance under the visible light

Lin Chen[a,c], Sudong Yang[a,b], Bin Hao[a,c], Jiongming Ruan[d], Peng-Cheng Ma[a,b,*]

[a] Laboratory of Environmental Science and Technology, The Xinjiang Technical Institute of Physics and Chemistry, Chinese Academy of Sciences, Urumqi 830011, China
[b] Key Laboratory of Functional Materials and Devices for Special Environments, Chinese Academy of Sciences, Urumqi 830011, China
[c] University of Chinese Academy of Science, Beijing 100049, China
[d] Department of Thermal Power Technology and Economic Operation, Huadian Electric Power Research Institute, Hangzhou 310030, China

ARTICLE INFO

Article history:
Received 30 September 2014
Received in revised form
17 November 2014
Accepted 20 November 2014
Available online 27 November 2014

Keywords:
TiO_2-based photocatalyst
Ag-AgBr
Glass fiber
Visible-light
Heterostructure

ABSTRACT

This paper reported the preparation of fiber-based plasmonic photocatalyst consisting of nano-scale Ag-AgBr, sub-micro TiO_2 and micro-scale glass fiber (GF). Various techniques were employed to study the morphology, structure and optical properties of the developed materials. The results showed that Ag-AgBr nanoparticles were highly dispersed on the surface of spherical TiO_2/GF, and the fibers exhibited a unique morphology of helical cracks along the fiber direction. The photocatalytic activities of obtained photocatalyst were evaluated by degrading methyl orange and phenol as model pollutants under the visible-light irradiation ($\lambda \geq 420$ nm). Inspiringly, the material exhibited wide absorption in the visible light and superior visible-light-driven photocatalytic activities compared with other TiO_2-based plasmonic photocatalysts. The improved photocatalytic performance was attributed to the synergistic effects arising from the hetero-junctions in the sample as well as the surface plasmon resonance of Ag nanoparticles. The integration of GF with plasmonic particles endowed the photocatalyst a high stability and reusability under the cyclic operations.

1. Introduction

Photocatalysis is regarded as a promising technology to solve the problems associated with the air and water pollution due to its strong oxidization capacity and environmental friendliness [1,2]. Since the pioneering work by Fujishima and Honda in 1972, significant progress has been made on the photocatalysis using titanium dioxide (TiO_2) [3]. However, TiO_2, a typical semiconducting material, has a band gap around 3.2 eV, and the activation of its photocatalytic capability requires ultraviolet (UV) light that contributes less than 5% of total energy of solar spectrum [4]. In addition, the low efficiency on separating electron–hole pairs in the material limits the practice of TiO_2 for wide photocatalytic applications [5]. To overcome these problems, many efforts have been devoted to modify the structure and composition of TiO_2 to enhance its visible light utilization, including doping with nonmetal materials [6,7], surface sensitization with organic dyes [8], coupling with narrow band gap semiconductors [9,10], and so on. Among various dopants, noble-metal nanoparticles (such as gold, silver, platinum) attracted much interest in recent years due to their surface plasmon resonance (SPR) phenomenon [11,12]. This unique property not only endows TiO_2 with improved absorption to visible light, but also facilitates the formation of Schottky barrier at the metal–TiO_2 interface, which acts as an electron trapper to suppress the recombination of photogenerated electron–hole pairs [13,14], thus enhancing the overall photocatalytic performance of TiO_2.

Silver halide (AgX, X = Cl, Br, I) is an important photosensitive material, and has been introduced into TiO_2-based photocatalysts for photocatalytic reactions with varying degree of success [15,16]. However, the photodecomposition of pure AgX reduces its activity under the light irradiation. Hybrid structure consisting of Ag nanoparticles and AgX (Ag-AgX) was developed as an alternative to address this issue. In this system, the Ag nanoparticles were generated on the surface of AgX, functioning as a protecting layer to improve the stability of AgX. The strong SPR effect of Ag nanoparticles also contributes greatly on the photoactivity of TiO_2 in the visible light region. For example, Hu et al. [17] prepared Ag-AgBr/TiO_2 using deposition–precipitation method, and the material showed an enhanced photocatalytic activity for the destruction of azo dyes under visible light. In another study, Tian

* Corresponding author at: Laboratory of Environmental Science and Technology, The Xinjiang Technical Institute of Physics and Chemistry, Chinese Academy of Sciences, Urumqi 830011, China. Tel.: +86 991 6992225.
E-mail address: mapc@ms.xjb.ac.cn (P.-C. Ma).

http://dx.doi.org/10.1016/j.apcatb.2014.11.044
0926-3373/

et al. reported [18] the controlled deposition of Ag-AgBr on TiO_2 tubes, and the developed photocatalyst showed strong degradation for phenol under the simulated solar-light irradiation.

Although Ag-AgBr/TiO_2 photocatalysts have been successfully prepared using different techniques, there are still many issues to be considered to optimize their structural, morphological, and photocatalytic properties for specific application. The collection and reusage of TiO_2-based photocatalysts in a slurry system become another major concern for their practical application [19,20]. Anchoring of TiO_2 nanoparticles onto suitable support offers an alternative for this problem. In this context, glass fiber (GF) is a promising candidate due to its characteristics of lightweight, low cost, transparency and high stability against light [21]. The fiber material can be processed into a variety of shapes (yarn, roven, fabrics, etc.), offering an advantage of easy operation when combining with different photocatalytic reactors.

Motivated by the above efforts, this paper reported the preparation of photocatalytic fibers decorated with micro-nano TiO_2 spheres using a solution route. Then the as-prepared TiO_2/GF was used as a support for loading plasmon Ag-AgBr nanocrystals, aiming at enhancing the photocatalytic capability of material using the visible light and stabilizing this property under the cyclic runs. The morphology, surface information and composition of fiber-based plasmonic photocatalyst were studied, and the photocatalytic activity of material was evaluated and compared with other TiO_2-based plasmonic photocatalysts.

2. Experimental

2.1. Raw materials

E-glass fibers with an average diameter of 12 μm were used in this study. The fibers were cleaned using acetone and then dried for application. Titanium tetrachloride ($TiCl_4$, 98%), silver nitrate ($AgNO_3$), potassium bromide (KBr), ammonium sulfate ($(NH_4)_2SO_4$), sulfuric acid (96%, H_2SO_4), ammonia water (28%, $NH_3{\cdot}H_2O$), polyvinylpyrrolidone (PVP, K30), ethylene glycol, and methyl orange (MO) were purchased from Tianjing Chemical Company, China. All chemicals were of analytical grade and used without further purification. Ultrapure water (Millipore, resistivity >18.5 MΩ cm) was used in all experiments.

2.2. Material preparation

2.2.1. Synthesis of TiO_2/GF

In a typical experiment, 1.5 g $(NH_4)_2SO_4$ was dissolved into 100 ml H_2SO_4 (0.01 mol/L). Then 1.0 mL of $TiCl_4$ was added dropwise into the solution under an ice bath. This was followed by the addition of 0.5 g GF into the mixture and heated at 95 °C for 3 h, yielding TiO_2/GF sample. The product was isolated from the solution by centrifugation and washed with water and ethanol for several times, and then dried in a vacuum oven at 60 °C for 3 h.

2.2.2. Synthesis of Ag-AgBr-TiO_2/GF photocatalyst

The preparation of Ag-AgBr-TiO_2/GF photocatalyst was achieved by mixing solutions consisting of precursors for AgBr and TiO_2/GF. Briefly, 0.12 g PVP and 0.035 g $AgNO_3$ were dissolved into 40 mL of ethylene glycol, then 0.55 g of TiO_2/GF was added into the mixture to obtain solution A. 0.024 g of KBr was added to another 20 mL of ethylene glycol to obtain solution B. Subsequently, solution B were added into solution A slowly and heated at 60 °C for 1.5 h. In order to avoid the photodecomposition of AgBr, the above experiments were conducted in a dark condition. After the reaction, the obtained product was collected by centrifugation, and washed with water. The sample was re-dispersed into 50 mL of water and irradiated under Xe lamp for 40 min with a change of solution color from transparency to slight gray, indicating the formation of Ag-AgBr-TiO_2/GF photocatalyst.

2.3. Photocatalytic tests

The photocatalytic activity of sample was evaluated by degrading MO under the visible light using a xenon lamp (300 W, PLS-SXE 300) with a cutoff filter at 420 nm. MO is a stable dye, and its photodegradation has been widely used to evaluate the performance of photocatalysts. A colorless organic dye, phenol (10 mg/L), was employed as another representative pollutant to exclude the contribution of dye-sensitized degradation during the photocatalytic reaction. In the experiment, 50 mg of photocatalyst was suspended in 100 ml of MO solution (10 mg/L) in a quartz reactor, which was equipped with inlet and outlet of water so that the heating effect to the solution due to the light can be minimized during the photocatalytic reaction. Prior to the irradiation, the suspension was stirred in the dark for 30 min to reach the adsorption-desorption equilibrium. Irradiation was located in the center of reactor, and at a given time interval, 3 mL of suspension was collected and the concentration of pollutants was determined by measuring their maximum absorbance (MO: 465 nm; Phenol: 269 nm) using a UV–Vis spectrophotometer (Shimadzu UV-2450). The total organic carbon (TOC), a parameter describing the mineralization of MO in solution, was also monitored using a TOC analyzer (Aopllo 9000).

2.4. Characterization

The crystal structure of samples was characterized on an X-ray diffractometer (XRD, Bruker D8) with Cu K_α radiation ($\lambda = 0.15$ nm). The morphology of photocatalyst was observed using a field-emission scanning electron microscope (SEM, Zeiss Supra55VP) and transmission electron microscope (TEM, JEOL JSM-2010). The elemental composition of sample was analyzed using an energy-dispersive X-ray detection system (EDX, Brucker X-Flash-SDD-5010) equipped in SEM. The chemical states of sample were analyzed by an X-ray photoelectron spectroscopy (XPS, PerkinElmer PHI 5000C). Diffuse reflectance spectroscopy (DRS) was performed on a spectrophotometer (SOLID 3700, Shimadzu) over the wavelength range of 300–800 nm. The photoluminescence (PL) characteristics of sample were probed on a fluorescence spectrophotometer (Hitachi F-4500).

3. Results and discussion

3.1. Structure and morphology of photocatalysts

The crystal structures of photocatalysts and corresponding precursors were characterized using XRD. The diffraction peak of pristine GF had a broad peak at $2\theta = 22°$ (Fig. 1A), representing

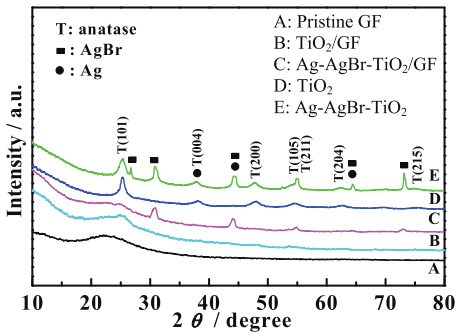

Fig. 1. XRD patterns of photocatalysts and corresponding precursors (A: Pristine GF; B: TiO_2/GF; C: Ag-AgBr-TiO_2/GF; D: TiO_2; E: Ag-AgBr-TiO_2).

the amorphous silica phase in GF. The TiO_2/GF sample exhibited an overlapped reflections from GF substrate and a peak at 26.1° (Fig. 1B), which was attributed to the anatase TiO_2 (JCPDS No.21-1272) [22]. The XRD pattern of Ag-AgBr-TiO_2/GF showed the presence of both TiO_2 and AgBr in the material (Fig. 1C). Besides the diffraction peaks assigned to the anatase TiO_2 (26.1°), the peak at 31.0° was attributed to the (2 0 0) crystal plane of AgBr [23]. The mean sizes of TiO_2 and AgBr on GF were 10.9 and 21.2 nm, according to the calculated results by separating the (1 0 1) plane of TiO_2 ($2\theta = 26.1°$) and (2 0 0) plane of AgBr ($2\theta = 31.0°$) using Rietveld refinement method [24]. To further verify the crystal states of nanoparticles on fiber surface, TiO_2 and Ag-AgBr-TiO_2 samples were prepared with absence of GF, and corresponding XRD spectra were compared with those deposited on fiber substrate. Several peaks ($2\theta = 25.4°$, 38.0°, 48.1°, 53.8°, 55.0°, 62.8°) attributed to the anatase TiO_2 were identified (D in Fig. 1), and their intensities were significantly higher than those from TiO_2/GF, further confirming that signals arising from GF overlapped those of TiO_2 on fiber surface. In contrast, the Ag-AgBr-TiO_2 sample exhibited peaks at 2θ values of 30.8°, 44.2°, 55.1°, 64.5° and 73.2°, matching very well with the diffraction peaks of (2 0 0), (2 2 0), (2 2 2), (4 0 0) and (4 2 0) planes of AgBr (JPCDS No. 06-0438, E in Fig. 1). Ag (1 1 1) facet at 37.8° (JCPDS No. 65-8428) was also observed in this sample and the diffraction peaks at 44.2°and 64.5° can be assigned to Ag^0 species (JCPDS No. 65-2871) and AgBr, respectively, while the characteristic peak of Ag^0 specie at 37.8° was overlapped with (0 0 4) plane of TiO_2 at $2\theta = 38.0°$ [25].

Various techniques were employed to characterize the surface information of Ag-AgBr-TiO_2/GF composites. The results from SEM (A-C in Fig. 2) showed that the fiber was decorated by spherical particles with diameter of 500–600 nm. The EDX results confirmed that the major elements in the sample were O, Si, Ti, along with trace amount of Ag and Br (Inset in Fig. 2B). The C was resulted from the carbon film for sample holding in SEM chamber. A close examination on the sample revealed that some smaller particles with an apparent size of 10–20 nm were anchored on the spherical particles (Fig. 2C), making the whole material be of hierarchical structures consisting of micro-scale fiber, sub-micron and nano-scale particles. The elemental mapping of sample clearly demonstrated the existence of titanium, sliver and bromine on fiber surface (D–F in Fig. 2), and the distribution of these elements was quite uniform. Qualitative analysis revealed that titanium exhibited the highest concentration on fiber surface, whereas the bromine showed the lowest one. It should be noted here that the silver exhibited a more pronounced signal on fiber than that of the bromine, suggesting the reduction of partly Ag^+ to Ag. These results along with morphology of sample indicated that TiO_2/GF can effectively function as a scaffold for the homogeneous anchoring of Ag-AgBr nano-hybrids. The generation of these nanoparticles was resulted from the presence of Ag^+ with assistance of PVP, ethylene glycol and KBr. During the synthesis of sample, PVP was adsorbed on Ag^+ surface, functioning as steric hindrance to kinetically control the growth rate of AgBr. The viscosity of ethylene glycol reduced the diffusion coefficients of both Ag^+ and Br^- ions to slow down the precipitation reaction, thus leading to a uniform distribution of AgBr on spherical TiO_2 particles (Fig. 2C). A fraction of Ag was embedded in the composites due to the photodecomposition of AgBr under the light irradiation [26].

An interesting observation on the sample is that the surface of GF shows helical cracks with spaced ran through the entire fiber length, and the pitch angles appear similar to one another (A and B in Fig. 2). The reason for this phenomenon may be due to the etching of GF by sulfuric acid. It is known that the metal ions (such as Al^{3+}, Mg^{2+}, Ca^{2+}) in GF can be leached out from the fiber surface. The mismatch between the outer surface and the intact inner core of fiber led to the shrinkage of surface. Since the shrinkage was restrained by the inner core, surface tensile stress was generated, causing helical crack formation on fiber surface [27,28].

To further investigate the crystal structures of material, the particles attached on GF were finely scratched from the fiber and characterized using TEM as a complementary technique. The TEM image revealed that the TiO_2 particle, which exhibited spherically in sub-micron (Fig. 3A), consisted of shallow spots surrounded by black nanocrystals (Fig. 3B). The result from high resolution TEM showed the appearance of three inter-planar spaces in the composites (Fig. 3C), i.e., the space of 0.228 nm corresponds to the (2 0 0) plane of AgBr, the one with 0.236 nm agrees with the (1 1 1) planes of Ag, and the inter-planar space of 0.354 nm is assigned to the (1 0 1) plane of anatase TiO_2. Therefore, it can be confirmed that hetero-junction consisting of anatase TiO_2 and plasmonic metal nanoparticles were formed in the sample, which provide the possibility to rectify the photocatalytic performance of composites under the visible light.

The chemical states of major elements on fiber surface were characterized by XPS. Fig. 4A shows the full XPS spectrum and elemental composition of material, confirming the existence of Ti, O, Ag, Br, C and Si in the sample (Fig. 4A). The C 1s signal at binding energy of 284.6 eV may be resulted from the adventitious hydrocarbon in XPS facility, whereas the binding energy of Si 2p at 103.0 eV originates from GF. The fine spectrum of Ti 2p shows two peaks at 458.7 eV and 464.3 eV (Fig. 4B), representing the Ti $2p_{3/2}$ and Ti $2p_{1/2}$ of Ti^{4+}, respectively [29]. The Ti $2p_{1/2}$ component is much broader than the Ti $2p_{3/2}$ peak, suggesting the shorter life of the former in the Ti^{4+} state. The Ag 3d spectrum consists of two individual peaks at 366.3 eV and 372.7 eV (Fig. 4C), which can be assigned to the $3d_{5/2}$ and $3d_{3/2}$ of either metallic Ag or Ag^+ ion. Each of these bands can be further deconvoluted into a pair of peaks (366.5/367.5 eV, 372.5/373.8 eV). The peaks at 367.5 eV and 373.8 eV can be attributed to the metallic Ag, whereas the peaks at 366.5 eV and 372.5 eV are from Ag^+ ion [30]. According to the areas covered by these deconvoluted peaks, the atomic ratio of Ag/Ag^+ in the sample was 1:11.5. This result suggested that a small quantity of Ag^+ ion was reduced to Ag metal in the sample, which was agreeable with the atomic concentration of Br in the sample from EDX analysis (Inset in Fig. 2B), as each Ag^+ can combine stoichiometrically with only one Br^- ion. The deconvolution of Br shows two peaks at 67.2 eV and 68.1 eV (Fig. 4D), corresponding to the Br $3d_{5/2}$ and Br $3d_{3/2}$ of AgBr [30]. The results also proved that the KBr, the bromide source for AgBr, was absence in the prepared sample.

3.2. Photocatalytic performance of photocatalyst

The photocatalytic performance of prepared photocatalyst and corresponding precursors was studied, and their capabilities to degrade MO were compared by introducing a degradation efficiency parameter, C/C_0, where C_0 and C are the initial and residual concentration of MO at different time intervals. Fig. 5A presents the variation of MO in the presence of different photocatalysts in the dark for 30 min and under the visible light irradiation. Negligible photodegradation of organic dye was observed with absence of photocatalyst, suggesting the decomposition of MO due to the photosensitization could be ignored basically. When pristine GF and TiO_2 powder were used as photocatalysts, only a slight photodegradation of MO was observed within 110 min, indicating the marginal sensitivity of materials to the visible light. In contrast, when Ag/AgBr-TiO_2/GF was employed as a photocatalyst, the peak at 465 nm gradually decreased with increasing irradiation time (Fig. S1A), and the orange color of MO in solution was faded and eventually became bleached after 110 min. The photocatalyst also performed strong degradation capability to phenol, a colorless organic material exhibiting no absorption in the visible range. The temporal evolution of the spectrum over the Ag/AgBr-TiO_2/GF

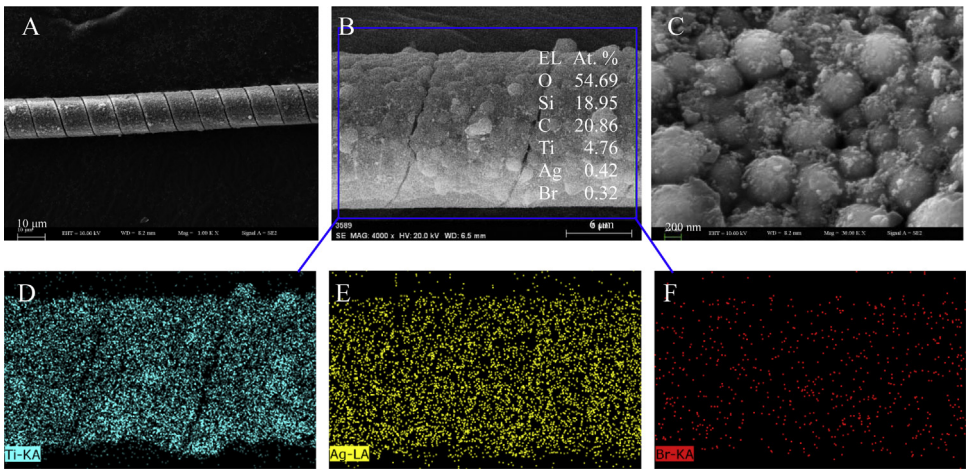

Fig. 2. Morphology of photocatalyst under the different magnifications (A–C) and composition mapping of major elements on fiber surface (D: Ti; E: Ag; F: Br).

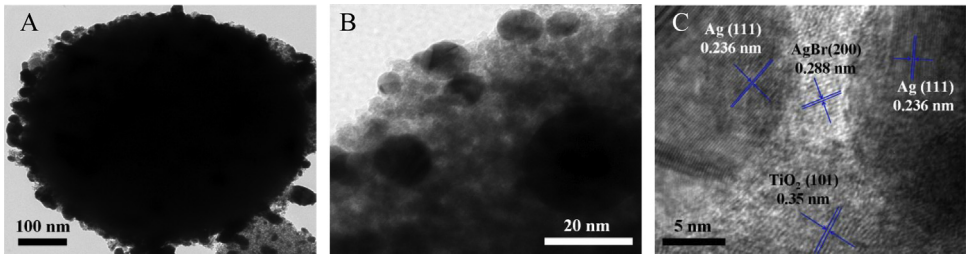

Fig. 3. TEM images showing the morphology of sub-micron and nano-scale particles on fiber surface.

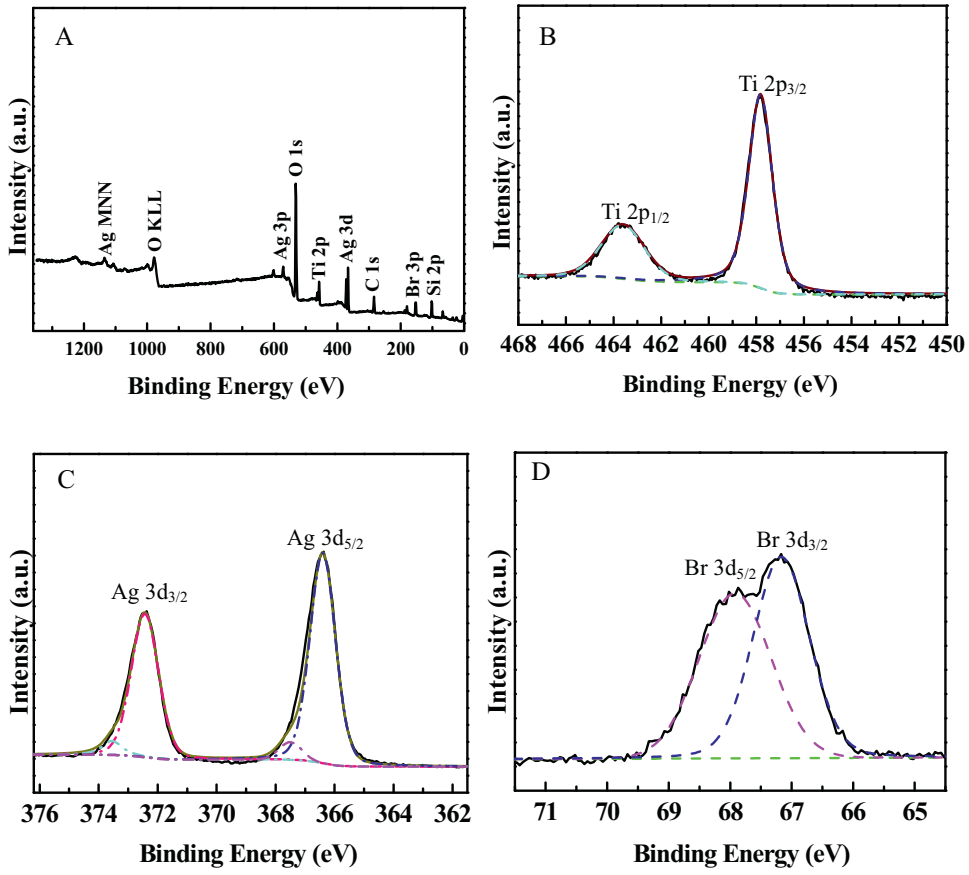

Fig. 4. General XPS spectrum of Ag-AgBr-TiO_2/GF composites (A) and the deconvolution of major elements Ti, Ag and Br (B–D).

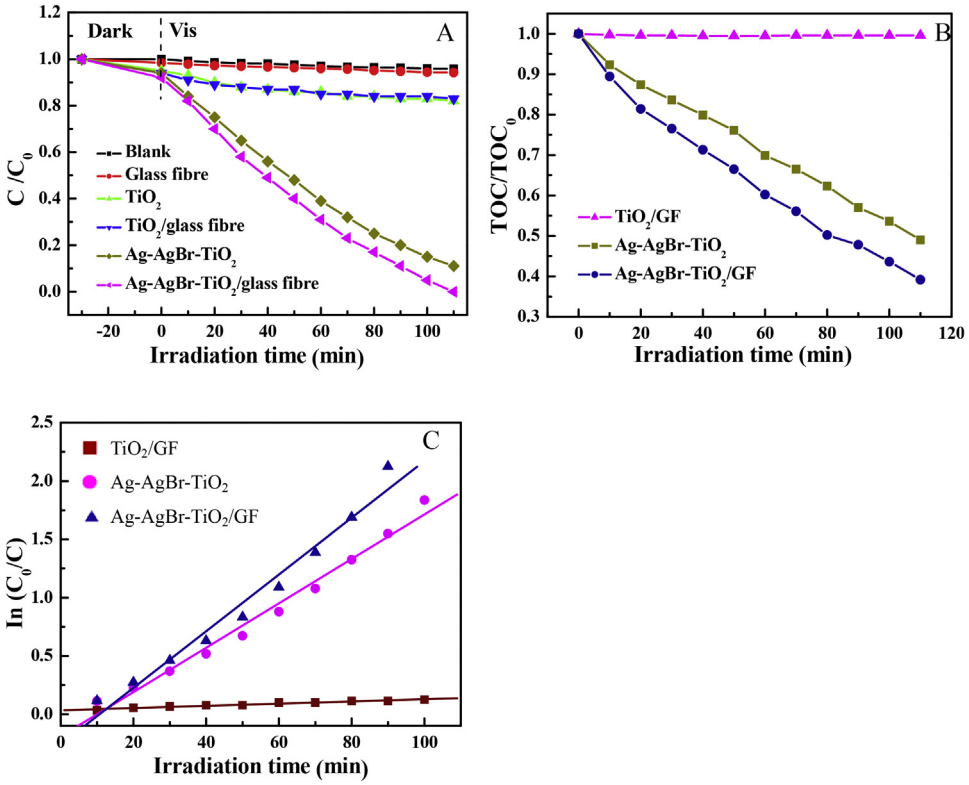

Fig. 5. Photocatalytic performance of different materials under the visible light (A and B: Variation on MO concentration and TOC as a function of irradiation time; C: Kinetic results showing the photodegradation capability of different photocatalysts).

showed a rapid decrease in the characteristic absorption of phenol at 269 nm under the visible light (Fig. S1B). This result confirmed that the dye-sensitization contributes marginally to the whole photocatalytic reaction. The distinctive enhancement observed in Ag/AgBr-TiO_2/GF may attribute to the synergistic effects arising from the surface plasmon resonance of Ag, the spherical TiO_2 particles and improved interactions between the photocatalytic particles and GF. This assumption was partly confirmed by the fact that nearly 88% of MO was decomposed when employing Ag-AgBr-TiO_2 nanocrystals in the photocatalytic reaction.

The study on the mineralization of organic pollutant in water using TOC analysis can provide evidence that the decoloration of organic dye is resulted from the photodegradation rather than the photosensitization or physical adsorption. Fig. 5B shows the evolution of TOC in solution using three typical photocatalysts. The results further confirmed the poor photoactivity of TiO_2/GF sample under the visible light, as negligible changes on TOC were observed. The concentration of TOC in solution was reduced by about 53% with presence of Ag-AgBr-TiO_2 after 110 min of light irradiation. When Ag-AgBr-TiO_2/GF sample was employed, the decrease on TOC reached approximately 62%, suggesting the highest mineralizing ability of this sample among the photocatalysts. These results are quite agreeable with those obtained by evaluating the decoloration of MO using UV–Vis spectrophotometer, and convincing that the photosensitization and physical adsorption have slight effect on the photocatalytic reaction. It should be noted here that the trend for TOC reduction was slower than that of the decolorization of MO. This can be explained by the fact that the results from the former analysis reflect the concentration of MO as well as organic materials decomposed at intermediate states as a whole.

The degradation kinetics for MO is also elaborated based on the decoloration of pollutant in solution, and the results are presented in Fig. 5C. It can be seen that the curves of $\ln(C/C_0)$ versus irradiation time were linear, indicating a good correlation to first-order reaction kinetically [31]. The determined rate constants of photocatalysis, k, were 0.001, 0.019 and 0.024 min^{-1} for TiO_2/GF, Ag-AgBr-TiO_2 and Ag-AgBr-TiO_2/GF, respectively. These quantitative results implied that the incorporation of plasmonic nanoparticles endows TiO_2 with positive response to the visible light, and this property was not affected by the introduction of GF in the photocatalyst.

The photocatalytic performance of the materials developed in this study was compared with those reported in the literature, targeting on the degradation of MO in water using TiO_2-based plasmonic photocatalysts (Table S1). While the rate constants (k values) varied depending on the preparation of materials and the experimental setups, it was obvious that the Ag-AgBr-TiO_2/GF photocatalyst exhibited a higher k than commercial P25 and rare-metal-contained TiO_2, and comparable to the AgX-TiO_2 photocatalysts [26,32–39]. It was worthwhile to mention that the concentration of photocatalyst in MO solution in the current study was 0.5 g/L, much lower than those reported by others ($\geq$1.0 g/L). Considering the weight content of TiO_2-based particles covered less than 20% in the sample (EDX results in Fig. 2B), the photocatalyst developed in this study had a unique advantage of maximizing the photocatalytic performance of plasmonic TiO_2 efficiently and effectively, and the GF offers the material to be easily recycled and reused, which will be discussed in the following section.

To have a better understanding on the enhanced photocatalytic property of Ag-AgBr-TiO_2/GF, it is advisable to study the semiconducting behavior of sample as the incorporation of heterogeneous atoms into TiO_2 may change this property dramatically. Fig. 6A shows the DRS of photocatalysts and corresponding analysis on their band-gaps. The absorption onset for TiO_2/GF was at 390 nm, agreeable with the intrinsic absorption of TiO_2 [40,41]. Compared with TiO_2/GF, the Ag-AgBr-TiO_2 exhibited strong absorption from 300 to 800 nm, especially in the visible light region (400–700 nm) where the former sample showed no response at all. This

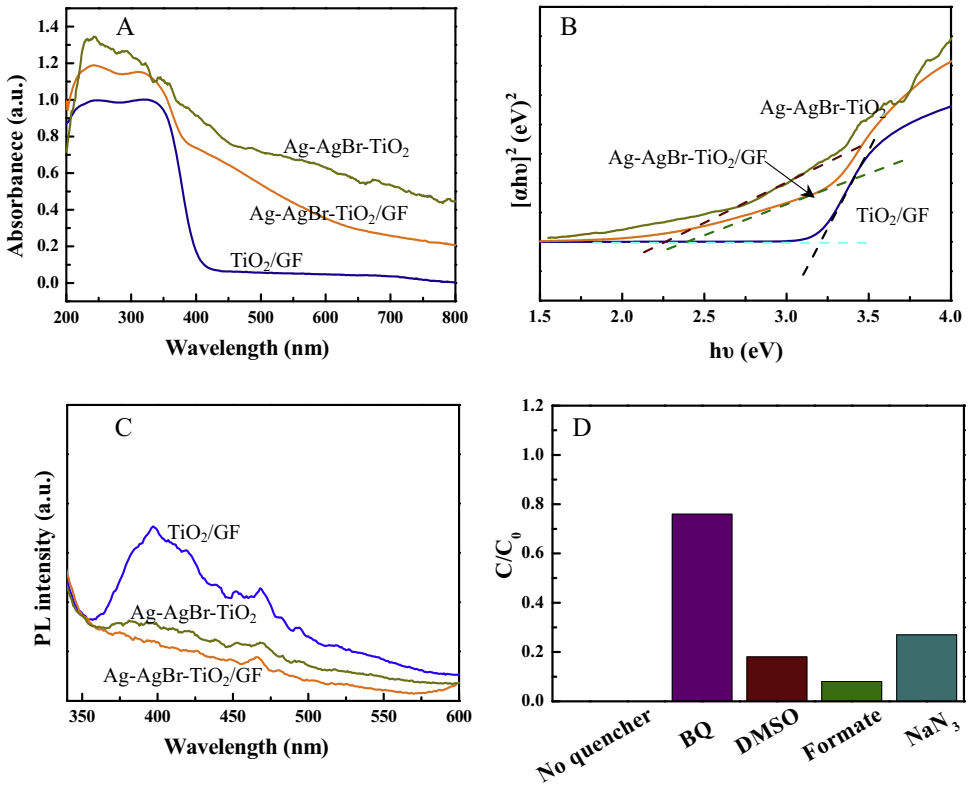

Fig. 6. DRS spectra (A) and corresponding determination on the band gaps of photocatalysts (B); (C) PL spectra of photocatalysts with an excitation wavelength of 325 nm; (D) Photocatalytic degradation of MO using Ag-AgBr-TiO_2/GF with the presence of various scavengers after 110 min of irradiation.

observation is resulted from the SPR of Ag nanoparticles and the visible-light absorption of AgBr which has an intrinsic band gap of 2.6 eV [12,17,18]. It is known that Ag nanoparticles exhibited localized surface plasmon resonance (LSPR) with a sharper peak in the visible light region (400–600 nm), however, this was not observed in this sample and Ag-AgBr-TiO_2/GF possibly due to the non-uniform size of Ag nanoparticles (Fig. 3B) as well as the dielectric environment of nanoparticles [42] accompanied by AgBr, TiO_2 and glass. The Ag-AgBr-TiO_2/GF sample shows a pretty similar DRS spectrum to that of Ag-AgBr-TiO_2, suggesting that the response of Ag-AgBr-TiO_2 to the visible light was not sacrificed by the introduction of glass material. By plotting the optical absorption data ($[\alpha h\upsilon]^2$) vs. photon energy ($h\upsilon$), the band-gap of samples were determined. The estimated band-gaps for TiO_2/GF, Ag-AgBr-TiO_2 and Ag-AgBr-TiO_2/GF were 3.17, 2.25 and 2.31 eV, respectively (Fig. 6B). The decreased band-gap in the Ag-AgBr-TiO_2/GF was resulted from the extension of visible-light absorption edge in the material. In other words, the photons with low energy (high wavelength) can stimulate the photocatalyst to generate electron–hole pairs, leading to a better photocatalytic performance of Ag-AgBr-TiO_2/GF under the visible light.

Light-generated electrons and holes are the two main species in governing the photocatalytic capability in semiconducting materials. The photoluminescence (PL) emission spectrum offers a powerful tool to understand this since the recombination of electron–hole can release energy in the form of fluorescence emission, and a lower fluorescence emission intensity implies a lower electron–hole recombination rate and a higher photocatalytic activity [43,44].

In order to investigate the separation rate of electron–hole pairs, the PL spectra of samples were measured in the wavelength range of 350–600 nm (Fig. 6C). Three major emission peaks locating at 403 nm (3.1 eV), 450 nm (2.6 eV) and 464 nm (2.7 eV) were observed in the TiO_2/GF sample. The strong emission peak at 403 nm was attributed to the intrinsic luminescence of TiO_2, originating from the photo-induced electron transfer between the valence band (VB) of O 2p to the conduction band (CB) of Ti 3d in TiO_2 [43]. The peaks at 450 nm and 464 nm were attributed to band edge free excitons in the sample. The two weak peaks at 482 nm and 492 nm were assigned to the bound excitons and surface defects in the samples. The PL peak intensity of Ag-AgBr-TiO_2/GF sample decreased significantly compared with that of TiO_2/GF. For example, the intrinsic luminescence arising from TiO_2 at 403 nm was absence in the sample. A possible reason for this observation was that the Ag-AgBr nano-hybrids anchored on TiO_2 acted as trapper to capture the photo-induced electrons, offering a separated pathway for their transfer, thus effectively inhibit the recombination of electron–hole pairs.

Trapping experiments were conducted in an effort to verify qualitatively the main active species during the photocatalytic process. Four reagents, including benzoquinone (BQ, $O_2\cdot^-$ scavenger), dimethyl sulfoxide (DMSO, ·OH scavenger), formate (h^+ scavenger) and sodium azide (NaN_3, $^1O_2$ scavenger), were employed and their effects on the photodegradation rate of MO were investigated (Fig. 6D). The results showed that nearly 75% of MO was remained in the solution with the addition of BQ, suggesting an effective trapping of $O_2\cdot^-$ radicals during the photocatalysis. In contrast, addition of DMSO, formate and NaN_3 caused slight reduction on the removal ratio of MO. According to these observations, it can be deduced that photo-excited radicals like ·OH, $O_2\cdot^-$, $^1O_2$ and holes (h^+) were produced and acted as reactive species over the Ag-AgBr-TiO_2/GF under the visible light, and $O_2\cdot^-$ was the most predominant reactive species in the system.

On the basis of aforementioned results, a possible mechanism for the visible-light-driven photocatalysis was proposed (Fig. 7). In the structure of Ag-AgBr-TiO_2/GF, Ag nanoparticles were in situ

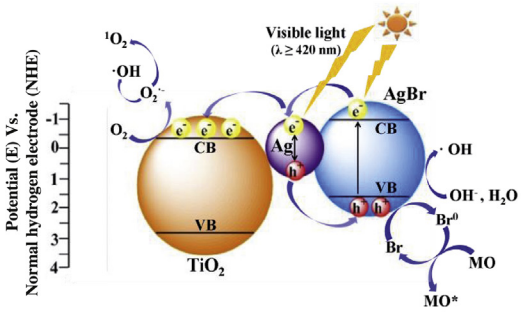

$$AgBr + h\nu \rightarrow AgBr(e^- + h^+) \quad (1)$$
$$Ag + h\nu \rightarrow Ag^* \quad (2)$$
$$Ag^* + TiO_2 \rightarrow TiO_2(e^-) + Ag^{+\bullet} \quad (3)$$
$$AgBr(e^- + h^+) + TiO_2 \rightarrow AgBr(h^+) + TiO_2(e^-) \quad (4)$$
$$TiO_2(e^-) + O_2 \rightarrow O_2^{\bullet -} + TiO_2 \quad (5)$$
$$O_2^{\bullet -} + H^+ \rightarrow HO_2^{\bullet} \quad (6)$$
$$HO_2^{\bullet} + TiO_2(e^-) + H^+ \rightarrow H_2O_2 + TiO_2 \quad (7)$$
$$H_2O_2 + TiO_2(e^-) \rightarrow {}^{\bullet}OH + OH^- + TiO_2 \quad (8)$$
$$O_2^{\bullet -} + {}^{\bullet}OH \rightarrow {}^1O_2 + OH^- \quad (9)$$
$$Ag^{+\bullet}/AgBr(h^+) + Br^- \rightarrow Ag/AgBr + Br^0 \quad (10)$$
$$Br^0 + MO \rightarrow MO^* + Br^- \quad (11)$$
$$O_2^{\bullet -}, {}^1O_2, AgBr(h^+), {}^{\bullet}OH + MO \rightarrow \text{mineralized products} \quad (12)$$

Fig. 7. Possible mechanism of photocatalytic reaction using Ag-AgBr-TiO_2/GF photocatalyst.

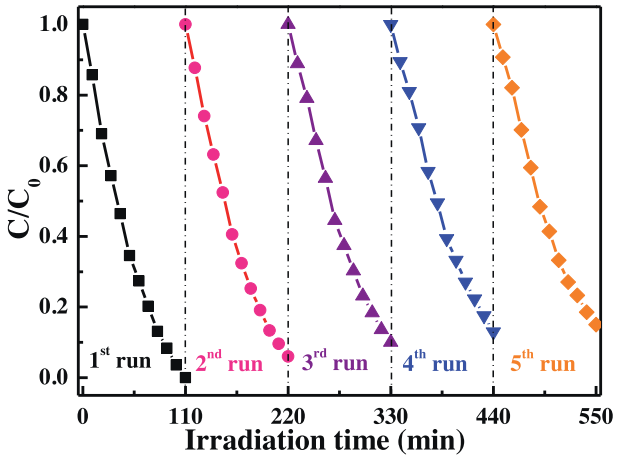

Fig. 8. Recyclability of the Ag-AgBr-TiO_2/GF photocatalyst for the degradation of MO under visible irradiation.

formed at the interface of TiO_2 and AgBr, favorable for the formation of nanoscale hetero-junctions in the sample. Under the visible light, Ag and AgBr can be simultaneously excited to generate a large amount of electron–hole pairs (Eqs. (1)–(2) in Fig. 7). The plasmon-induced electrons on Ag nanoparticles flowed preferably to the CB of TiO_2 rather than AgBr, owing to the less negative CB edge of TiO_2 (−0.10 V vs. NHE) as compared to that of AgBr (−1.04 V vs. NHE). Besides, the electrons from the photo-excited AgBr could be injected into the Ag, which could prevent the Ag corrosion and result in a rather stable system. The electrons in this state has a high possibility to interact with molecular oxygen adsorbed on TiO_2, resulting in the formation of oxygen-contained radicals, such as $O_2{\cdot}^-$, $HO_2{\cdot}$, ·OH, OH^-, $^1O_2$ (Eqs. (5)–(9) in Fig. 7). Consequently, the mineralization of MO was triggered by these highly active species in solution. On the other hand, the photo-produced holes in the VB of AgBr could oxidize Br^- ion to Br^0, and this process was further enhanced due to the diffusion of holes from Ag nanoparticles to the surface of AgBr (Eq. (10) in Fig. 7). It is known that elementary Br^0 is chemically reactive and can effectively oxidize organic material adsorbed on the surface of photocatalyst and simultaneously be reduced to Br^- (Eq. (11) in Fig. 7) [45]. The reduced Br^- was subsequently combined by Ag^+ to regenerate AgBr (Eq. (10) in Fig. 7). The holes located on the surface of AgBr have additional capability to combine with water molecules either adsorbed on the photocatalyst or in solution, yielding ·OH radicals in the system. The different pathways for the transfer of electrons and holes make it possible to separate them efficiently from recombination, thus enhance the overall photocatalytic performance of Ag-AgBr-TiO_2/GF.

In addition to the photocatalytic activity, the stability and recyclability of photocatalyst were important issues for their practical applications. The changes in the degradation behavior of MO under cyclic operations using Ag-AgBr-TiO_2/GF are presented in Fig. 8. The results showed that the efficiency of photocatalyst was as high as 100% for the first cycle and remains above 85% even after five cycles, demonstrating the unique advantage of using GF in stabilizing and recycling the plasmonic particles for photocatalytic application. The excellent recyclability of material also proved that the final removal of MO from solutions was dominated by the photocatalytic process rather than the physical adsorption. The slight decrease on the activity during the repeated runs was thought to be the loss of the catalyst during the photocatalytic trials [46]. Anyway, the remained high performance of the fiber-based photocatalysts under cyclic runs along with their easy separation from solution guarantees their applicable and continuous photocatalysis in liquid media.

4. Conclusions

In summary, fiber-based plasmonic photocatalyst (Ag-AgBr-TiO_2/GF) was prepared by a combined process by depositing AgBr nanoparticles onto TiO_2/GF and a following reduction of Ag^+ to Ag^0 species. The developed photocatalyst exhibited enhanced photocatalytic performance than Ag-AgBr-TiO_2 and TiO_2-based plasmonic photocatalysts over the degradation of MO under the visible light. The mechanisms behind this enhancement were three-folds: (i) the more interfacial active sites and hetero-junctions formed in the hierarchical structures of sample, (ii) the enhanced absorption of visible light due to the SPR effects of Ag nanoclusters generated in situ in the sample, and (iii) the synergistic effects arising from Ag, AgBr and TiO_2 substances for effective separation of photo-generated electrons and holes. Anchoring Ag-AgBr-TiO_2 particles on fiber substrate offers a cost-effective way to remove organic pollutants in water, as verified by the maximization on the photocatalytic performance of plasmonic particles as well as the excellent recyclability of photocatalyst under the cyclic operations.

The technique and findings established in this study also showed some potential applications for environmental remediation and personal healthcare protection. It is known that Ag-AgBr is a light-sensitive material with excellent anti-bacterial capability [47,48], whereas TiO_2 is an environmental-benign and non-toxic substance commonly used in food and cosmetic products. The combination of these nanoparticles with traditional micro-scale fibers endows the later with multi-functionalities, which can be employed to degrade volatile organic compounds (VOCs) for indoor air quality control. In addition, the prototype fibers can be processed to breathing masks for the purpose of anti-PM2.5 particles in air. Further optimization and evaluation on the reliability of these materials will be the subject for our forthcoming reports.

Acknowledgements

This project was supported by the Western Light Program (Project No. RCPY201103) of Chinese Academy of Sciences, the 1000-Talent Program (Recruitment Program of Global Expert, In Chinese: Qian-Ren-Ji-Hua), as well as the Program for Attracting High-level Talents in Xinjiang Uyghur Autonomous Region.

Appendix A. Supplementary data

Supplementary data associated with this article can be found, in the online version, at http://dx.doi.org/10.1016/j.apcatb.2014.11.044.

References

[1] X.B. Chen, S.H. Shen, L.J. Guo, S.S. Mao, Chem. Rev. 110 (2010) 6503–6570.
[2] P. Christopher, H.L. Xin, S. Linic, Nat. Chem. 3 (2011) 467–472.
[3] A. Fujishima, K. Honda, Nature 238 (1972) 37–38.
[4] C.M. Teh, A.R. Mohamed, J. Alloy Compd. 509 (2011) 1648–1660.
[5] C.H. An, S. Peng, Y.G. Sun, Adv. Mater. 22 (2010) 2570–2574.
[6] S. In, A. Orlov, R. Berg, F. Garcia, S.P. Jimenez, M.S. Tikhov, D.S. Wright, R.M. Lambert, J. Am. Chem. Soc. 129 (2007) 13790–13791.
[7] R. Asahi, T. Morikawa, T. Ohwaki, K. Aoki, Y. Taga, Science 293 (2001) 269–271.
[8] D. Duonghong, E. Borgarello, M. Gratzel, J. Am. Chem. Soc. 103 (1981) 4685–4690.
[9] J. Luo, L. Ma, T. He, C.F. Ng, S. Wang, H. Sun, H.J. Fan, J. Phys. Chem. C 116 (2012) 11956–11963.
[10] H. Wang, Y. Bai, H. Zhang, Z. Zhang, J. Li, L. Guo, J. Phys. Chem. C 114 (2010) 16451–16455.
[11] P. Wang, B.B. Huang, X.Y. Qin, X.Y. Zhang, Y. Dai, J.Y. Wei, M.H. Whangbo, Angew. Chem. Int. Ed. 47 (2008) 7931–7933.
[12] K. Fuku, R. Hayashi, S. Takakura, T. Kamegawa, K. Mori, H. Yamashita, Angew. Chem. Int. Ed. 29 (2013) 7446–7450.
[13] P. Wang, B.B. Huang, X.Y. Zhang, X.Y. Qin, Y. Dai, J. Zhan, J.X. Yu, H.X. Liu, Z.Z. Lou, Chem. Eur. J. 16 (2010) 10042–10047.
[14] M.R. Elahifard, S. Rahimnejad, S. Haghighi, M.R. Gholami, J. Am. Chem. Soc. 129 (2007) 9552–9553.
[15] Y.Q. Wang, L. Sun, B. Fugetsu, J. Mater. Chem. A 1 (2013) 12536–12544.
[16] H. Fan, J.Y. Zhu, J.C. Sun, S.X. Zhang, S.Y. Ai, Chem. Eur. J. 19 (2013) 2523–2530.
[17] C. Hu, Y. Lan, J. Qu, X. Hu, A. Wang, J. Phys. Chem. B 110 (2006) 4066–4072.
[18] G. Tian, Y. Chen, H.L. Bao, X. Meng, K. Pan, W. Zhou, C. Tian, J.Q. Wang, H. Fu, J. Mater. Chem. 22 (2012) 2081–2088.
[19] M. Bideau, B. Claudel, C. Dubien, L. Faure, H. Kazouan, J. Photochem. Photobiol. A 91 (1995) 137–144.
[20] W.A. Daoud, S.K. Leung, W.S. Tung, J.H. Xin, K. Cheuk, K. Qi, Chem. Mater. 20 (2008) 1242–1244.
[21] L. Chen, S.D. Yang, E. Mäder, P.C. Ma, Dalton Trans. 43 (2014) 12743–12753.
[22] J.B. Zhou, Y. Cheng, J.G. Yu, J. Photochem. Photobiol. A 223 (2011) 82–87.
[23] W.S. Choi, G.Y. Byun, T.S. Bae, H.J. Lee, ACS Appl. Mater. Interfaces 5 (2013) 11225–11233.
[24] P. Wang, B.B. Huang, X. Zhang, X. Qin, H. Jin, Y. Dai, Z. Wang, J. Wei, J. Zhan, S. Wang, J. Wang, M.H. Whangbo, Chem. Eur. J. 15 (2009) 1821–1824.
[25] W. Jiao, N. Li, L.Z. Wang, L. Wen, F. Li, G. Liu, H.M. Cheng, Chem. Commun. 49 (2013) 3461–3463.
[26] D.S. Wang, Y.D. Duan, Q.Z. Luo, X.Y. Li, J. An, L.L. Bao, L. Shi, J. Mater. Chem. 22 (2012) 4847–4854.
[27] A.G. Metcalfe, M.E. Gulden, G.K. Schmitz, Glass Technol. 12 (1971) 15–23.
[28] M.M. Shokrieh, N. Nasir, H. Karimipour, J. Compos. Mater. 46 (2012) 765–772.
[29] Y.H. Zhang, Z.R. Tang, X.Z. Fu, Y.J. Xu, Appl. Catal. B: Environ. 3–4 (2011) 445–452.
[30] P. Wang, B.B. Huang, X. Qin, X. Zhang, Y. Dai, M.H. Whangbo, Inorg. Chem. 48 (2009) 10697–10702.
[31] Y. Li, H. Zhang, Z. Guo, J. Han, X. Zhao, Q. Zhao, S.J. Kim, Langmuir 24 (2008) 8351–8357.
[32] M.S. Hamdy, W.H. Saputera, E.J. Groenen, G. Mul, J. Catal. 310 (2014) 75–83.
[33] Y. Yang, G.Z. Wang, Q. Deng, D.H.L. Ng, H.J. Zhao, ACS Appl. Mater. Interfaces 6 (2014) 3015–3022.
[34] R. Liu, P. Wang, X.F. Wang, H.G. Yu, J.G. Yu, J. Phys. Chem. C 116 (2012) 17721–17728.
[35] Z.D. Meng, L. Zhu, J.G. Choi, M.L. Chen, W.C. Oh, J. Mater. Chem. 21 (2011) 7596–7603.
[36] S. Oros-Ruiz, R. Gomez, R. Lopez, A. Hernandez-Gordillo, J.A. Pedraza-Avella, E. Moctezuma, E. Perez, Catal. Commun. 21 (2012) 72–76.
[37] J. Cao, B.Y. Xu, B.D. Luo, H.L. Lin, S.F. Chen, Appl. Surf. Sci. 257 (2011) 7083–7089.
[38] Q.Y. Li, Y.Y. Xing, R. Li, L.L. Zong, X.D. Wang, J.J. Yang, RSC Adv. 2 (2012) 9781–9785.
[39] Y.J. Zang, R. Farnood, Appl. Catal. B: Environ. 79 (2008) 334–340.
[40] L. Kuai, B. Geng, X. Chen, Y. Zhao, Y. Luo, Langmuir 26 (2010) 18723–18727.
[41] X.B. Chen, C. Burda, J. Am. Chem. Soc. 15 (2008) 5018–5019.
[42] T.R. Jensen, M.D. Malinsky, C.L. Haynes, R.P. Van Duyne, J. Phys. Chem. B 104 (2000) 10549–10556.
[43] N. Lakshminarasimhan, E. Bae, W. Choi, J. Phys. Chem. C 111 (2007) 15244–15250.
[44] T.J. Sun, J.S. Qiu, C.H. Liang, J. Phys. Chem. C 112 (2008) 715–721.
[45] Y. Sang, L. Kuai, C.Y. Chen, Z. Fang, B.Y. Geng, ACS Appl. Mater. Interfaces 6 (2014) 5061–5068.
[46] M. Zahmakıran, S. Özkar, Appl. Catal. B: Environ. 89 (2009) 104–110.
[47] H.F. Cheng, B.B. Huang, P. Wang, Z.Y. Wang, Z.Z. Lou, J.P. Wang, X.Y. Qin, X.Y. Zhang, Y. Dai, Chem. Commun. 47 (2011) 7054–7056.
[48] H. Shi, G. Li, H. Sun, T. An, H. Zhao, P.K. Wong, Appl. Catal. B: Environ. 158–159 (2014) 301–307.